

Gold Nanoparticle Assemblies by Metal Ion–Pyridine Complexation and Their Rectified Quantized Charging in Aqueous Solutions

Shaowei Chen,* Renjun Pei, Tongfeng Zhao, and Daniel J. Dyer

Department of Chemistry, Southern Illinois University, Carbondale, Illinois 62901-4409

Received: September 19, 2001; In Final Form: December 17, 2001

Gold nanoparticle assemblies were constructed by exploiting the complexation interactions between divalent metal ions and pyridine moieties. The thickness (layers) of the particle thin films was readily controlled by the repetition of the alternate dipping cycles, as monitored by quartz crystal microbalance (QCM). Electrochemical studies of these surface-immobilized nanoparticle layers revealed rectified quantized charging characters in aqueous solutions in the presence of hydrophobic anions. The effects of the nature of the electrolyte ions were investigated in the context of their hydrophobicity and interactions with the surface-bound particle molecules. It was found that the onset voltammetric potentials, as well as the effective molecular capacitance of the nanoparticles, were sensitive to the solution compositions. The behaviors were quite similar to those with the nanoparticle assemblies fabricated by dithiol linkages. The present study provided additional experimental parameters that could be used for the manipulation of nanoscale electron transfer.

Introduction

Recently, we discovered that the quantized capacitance charging of monolayer-protected nanoparticles could be rectified by some unique electrolyte ions in aqueous solutions, a behavior that differed drastically from those observed in organic media.¹ The responses have been interpreted on the basis of a Randles equivalent circuit, where the formation of particle/ion pairs led to the manipulation of the electrode interfacial double layers and hence the different charging responses at positive and negative potentials. Additionally, it was found that these charging features evolved from those similar to conventional molecular diodes to those of quantized charging rectifiers, a transition effected in the presence of electrolyte anions of increasing hydrophobicity. These unique characters might pave the way toward the development of nanoparticle-based single-electron molecular diodes.

In these previous studies,^{1,2} the nanoparticle monolayers were constructed by using a two-step procedure involving surface exchange reactions with alkanedithiols followed by self assembly. Here, the nanoparticles were first exchanged with alkanedithiols of similar chain lengths rendering the nanoparticles surface active with various copies of peripheral thiol groups. These then served as the anchoring sites for particle surface assembling, akin to monomeric alkanedithiols. Various other efficient routes for nanoparticle surface organization have also been reported,³ which generally exploit bifunctional ligands to bridge the particles onto the substrate surfaces. For instance, the strong binding of divalent transition metal ions to carboxylate moieties has been used to fabricate monolayers as well as multilayers of nanoparticle molecules.^{3a} The nanoparticle film thickness (layers) can be easily manipulated by the cycles of alternate dipping of the substrates into solutions of the complexing ions and the nanoparticles.

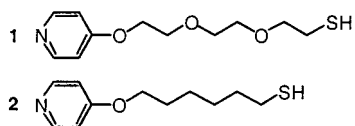
In this report, we first describe the fabrication of gold nanoparticle surface thin films by taking advantage of the strong

complexation interactions between transition metal ions and pyridine functional groups. These then serve as the structural basis in the investigation of ion-induced rectification of nanoparticle quantized charging, in which effects of the metal centers on the electrolyte ion binding will be examined. The electrochemistry of these surface-immobilized nanoparticle assemblies exhibits well-defined rectified quantized charging features in aqueous solutions, which are found to be sensitive to the electrolyte compositions as well as concentrations. The responses are quite similar to those with the nanoparticle assemblies fabricated by dithiol linkages.^{1,2} However, the ion-binding chemistry appears to be more complicated where greater deviation from theoretical prediction is observed at higher charged states of nanoparticles, presumably because of the interactions between electrolyte ions and the metal centers. The nanoparticle assemblies described here can then be easily removed from the electrode surface by incubating the modified electrodes into an EDTA solution. This provides a simple control of these single-electron current rectifiers.

Experimental Section

Chemicals. 1-Octanethiol (C8SH, 97%, ACROS), ethylenediaminetetraacetic acid (sodium salt, EDTA, 99+%, Aldrich), ammonium hexafluorophosphate (NH₄PF₆, 99.5%, ACROS), potassium hexafluorophosphate (KPF₆, 99%, ACROS), ammonium perchlorate (NH₄ClO₄, 99.8%, ACROS), ammonium tetrafluoroborate (NH₄BF₄, 97%, ACROS), tetramethylammonium nitrate (TMANO₃, ACROS), tetramethylammonium tetrafluoroborate (TMABF₄, 97%, ACROS), tetraethylammonium nitrate (TEANO₃, 99%, ACROS), tetraethylammonium hexafluorophosphate (TEAPF₆, 99%, Aldrich), tetraethylammonium perchlorate (TEAP, Pfaltz & Bauer), and tetra-*n*-butylammonium perchlorate (TBAP, ACROS) were all used as received. Potassium nitrate (KNO₃, Fisher) and ammonium nitrate (NH₄NO₃, Fisher) were both recrystallized twice from water prior to use. All solvents were obtained from typical commercial sources and used as received as well. Water was supplied by a Barnstead Nanopure water system (18.3 MΩ). The synthesis

* To whom correspondence should be addressed. E-mail: schen@chem.siu.edu.

SCHEME 1: Structures of Pyridine-Terminated Thiols

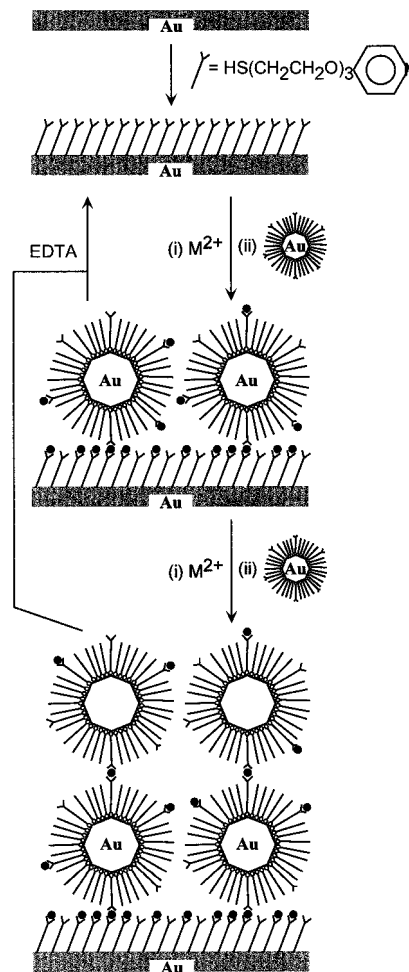
and characterization of pyridine-terminated thiol derivatives, 4-(1,4,7-trioxo-9-mercaptononyl)pyridine (**1**) and 4-(1-oxo-7-mercaptohexyl)pyridine (**2**) (Scheme 1), were described in the Supporting Information.

Nanoparticles. 1-Octanethiolate-protected gold (C8Au) nanoparticles were synthesized by the Schiffrin route.⁴ The particles were then fractionated by using a solvent and nonsolvent mixture (e.g., toluene and ethanol) to narrow the size dispersity with the final average particle core diameter ca. 2.0 nm (determined by transmission electron microscopic measurements) and then underwent a thermal annealing process by refluxing in toluene for 8 h, resulting in mostly spherical shape and monodisperse size.⁵ Further surface functionalizations were achieved by exchange reactions with a calculated feeding ratio of the C8Au particles and the pyridine-terminated thiol ligands (**1** or **2**). The final surface concentration is, *on average*, 11 pyridine moieties and 80 octanethiolate ligands (as characterized by ¹H NMR spectroscopy) with the resulting particles denoted as C8PyAu-1 and C8PyAu-2, respectively.

Nanoparticle Assemblies. The protocol for particles self-assembling onto a gold electrode surface is similar to the layer-by-layer deposition approach (Scheme 2). Briefly, a gold disk electrode (sealed in a glass tubing) was polished with 0.05 μm Al_2O_3 slurries and sonicated in dilute HNO_3 , H_2SO_4 , and Nanopure water, subsequently. The electrode was then dried in a gentle nitrogen stream and incubated in an ethanolic solution of pyridine thiols (**1** or **2**, 1 mM) for 24 h. This electrode was then removed from the solution, rinsed with copious ethanol, and dried again with a gentle nitrogen stream. The electrode was then immersed into an ethanolic solution of 0.1 M $\text{Cu}(\text{NO}_3)_2$ for 1 h, rinsed with ethanol, and then soaked in the gold particle solutions prepared in a binary mixture of ethanol and dichloromethane (1:1 v/v) for 4 h. Finally, the electrode was rinsed again with copious CH_2Cl_2 to remove loosely bound particle molecules and dried in a nitrogen stream before being transferred to an electrolyte solution cell for electrochemical measurements. By incubating the nanoparticle-coated electrodes in 0.05 M EDTA in water for 3 h (and then rinsing with CH_2Cl_2), the particle molecules were effectively removed from the surfaces, as monitored by QCM measurements.

Electrochemical and Quartz Crystal Microbalance Studies. Electrochemical and QCM measurements were carried out with a CHI440 Electrochemical Workstation. In aqueous solutions containing varied electrolytes, the reference electrode was calibrated with the redox potential of $\text{K}_3\text{Fe}(\text{CN})_6/\text{K}_4\text{Fe}(\text{CN})_6$. In organic solutions, a quasi-reference Ag/AgCl wire was used instead. The electrolyte solutions were prepared in water or in methylene chloride depending upon the specific electrolytes. The solutions were deaerated for at least 20 min prior to data acquisition by high-purity nitrogen, which was saturated by either water or methylene chloride and blanketed with an atmosphere of N_2 during the entire experimental procedure.

For the QCM measurements, the quartz crystals (from International Crystal Manufacturing) were made from polished quartz plates with a resonant frequency of 8 MHz and the crystal diameter of 14 mm. Ten nanometers of Cr was first deposited onto the center of the quartz crystals (dia. 5 mm), followed by 100 nm of gold. The crystals were subjected to UV-ozone

SCHEME 2: Procedure for Nanoparticle Assembling by the Chelating Interactions between Divalent (Transition) Metal Ions and Pyridine Moieties

cleaning (UVO cleaner model 42, Jelight Co.) for 15 min prior to immersion into the thiol solution for monolayer coating. The number of nanoparticle layers was varied by the number of alternate dipping cycles as described above. The frequency shift was measured in air where the crystals had been rinsed with copious solvents (ethanol and CH_2Cl_2) and dried in a gentle nitrogen stream.

Results and Discussion

Nanoparticle Assemblies. The assembling of nanoparticle surface layers was effected by virtue of the strong interactions between divalent ions of transition metals and pyridine moieties (Scheme 2). The thickness (i.e., number) of the nanoparticle layers can be controlled simply by the repetition of the dipping cycles where the uptake of each dipping process is monitored by QCM. Figure 1 shows the variation of quartz crystal frequency with the number of dipping cycles using Cu^{2+} ions as the binding centers and **1** as the chelating bridge, where one can see that the frequency change (relative to the frequency where the crystals are only coated with the pyridine monolayers) increases linearly with the number of dipping cycles. This indicates the reproducible deposition of nanoparticles during the dipping process. From the slope, one can see that for each layer of nanoparticles deposited onto the electrode surface, the quartz crystal frequency exhibits a decrease of 195 Hz. Using the Saubrey equation,⁶ the nanoparticle monolayer surface coverage can be evaluated to be $1.35 \mu\text{g}/\text{cm}^2$, that is, $1.08 \times$

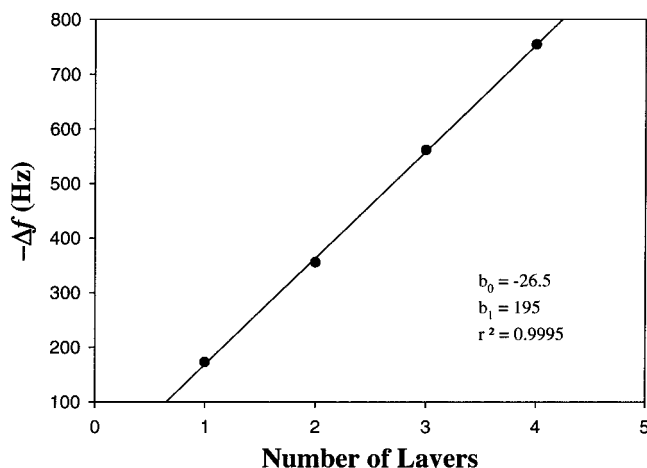


Figure 1. QCM frequency variation with the number of dipping cycles. The frequency change is relative to the frequency at which the crystals are coated only with the pyridine monolayers. The line is linear regression.

10^{13} particles/cm², by adopting a truncated octahedron core configuration^{4b,c} (and hence a particle composition of Au₃₁₄-(SR)₉₁). Assuming a close-packed hexagonal distribution of the surface-immobilized particles, the interparticle (center-to-center) distance is about 3.3 nm. This is even somewhat smaller than the particle physical diameter (core + two protecting ligands, which is about 4 nm). This discrepancy most likely reflects the formation of (partial) multilayer structures, as speculated previously,^{3a} where some of the Cu²⁺ ions originally adsorbed to the **1**-monolayer might be desorbed in the second dipping step and bridge **1**-functionalized gold nanoparticles on the electrode surface. Additionally, there might be oversimplification that the frequency change is solely due to the uptake of nanoparticles; adsorption of counterions and associated trace solvent molecules might have to be taken into account as well.

The ion-chelated nanoparticle assemblies can be easily eliminated by immersing the electrode into an EDTA solution where the divalent metal ions are removed from the particle assemblies to complex with EDTA molecules. This desorption process can again be monitored by QCM. For instance, the total frequency decrease after four dipping cycles is about 755 Hz (Figure 1), and after immersing the electrode into a 0.05 M EDTA solution for 3 h, the frequency that was measured subsequently shows an increase of 741 Hz, indicating almost complete removal of the nanoparticle molecules.

These studies demonstrate that the deposition of nanoparticle layers based on Cu²⁺/pyridine chemistry and the subsequent removal by EDTA is very effective. We also carried out studies with other metal divalent ions, such as Zn²⁺, Mn²⁺, and Ni²⁺. However, the surface coverages of nanoparticles are all quite low and hard to reproduce. Additionally, nanoparticle assemblies based on ligand **2** did not show a high surface coverage either. This is somewhat puzzling and suspected to result from the discrepancy of the surface conformations between these two monolayers. Thus, next we will focus only on the nanoparticle assemblies based on ligand **1**. Certainly further studies are desired to investigate the effects of surface structures on nanoparticle assembling.

Rectified Quantized Charging. Recently, we discovered that in aqueous solutions containing bulky and hydrophobic ions, nanoparticle surface assemblies exhibited rectified quantized charging features.¹ The behaviors were interpreted based on a Randles equivalent circuit where the binding of hydrophobic ions to the surface-immobilized MPC molecules leads to the

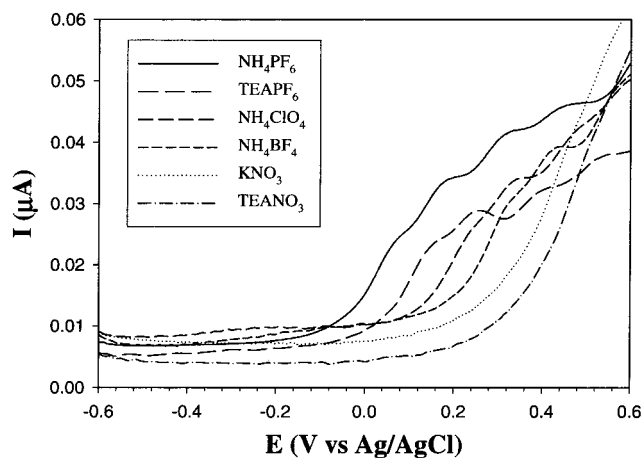


Figure 2. Representative differential pulse voltammograms (DPVs) of a monolayer of gold (C8PyAu-1) nanoparticles anchored to the electrode surface by Cu²⁺/pyridine chelating in varied electrolytes. All electrolyte concentrations were 0.10 M. The dc potential ramp was 20 mV/s, the pulse amplitude was 50 mV, and the pulse width was 200 ms.

manipulation of the electrode interfacial double layers. Similar responses are observed here. Figure 2 shows some representative differential pulse voltammograms (DPVs) of a monolayer of gold nanoparticles (C8PyAu-1) anchored to the electrode surface by Cu²⁺/pyridine complexation. In the presence of hydrophobic electrolyte anions, such as PF₆⁻, ClO₄⁻, BF₄⁻, etc., one can see a series of discrete electron-transfer processes in the positive potential regime, which are ascribed to the quantized charging to the nanoparticle molecules. In contrast, in the negative potential region, the voltammetric currents are significantly suppressed. These responses are akin to a current rectifier where the single-electron transfers are regulated by these “soft” anions.¹

However, in the presence of “hard” anions (e.g., NO₃⁻), the voltammetric responses are similar to a Coulomb blockade (Figure 2). At potentials more negative than the threshold potential (i.e., the onset potential,^{1b} E_{on}), the voltammetric currents are very small, whereas at potentials more positive than E_{on} , the current increases significantly with no apparent quantized charging characters. This behavior is similar to that of conventional molecular diodes. The discrepancy of voltammetric responses in solutions containing “soft” and “hard” ions is consistent with the ion binding mechanism proposed earlier.^{1b} This observation also strongly suggests that a transition from conventional molecular diodes to single-electron rectifiers can be effected by increasing the hydrophobicity of electrolyte ions. One might also note that bulky cations (TMA⁺ and TEA⁺) failed to initiate the quantized charging processes, in contrast to the anionic counterparts. As speculated previously,¹ this was attributed to the difference in their solvation structures and the interactions with the surface-bound particle molecules (more details below).

Table 1 lists the onset potentials in varied electrolyte solutions. One can see that as observed previously,^{1b} the onset potential exhibits a cathodic shift with anions of increasing hydrophobicity. Also, one can see that the onset voltammetric potentials can be grouped into the following sequence: (NH₄PF₆, KPF₆, TEAPF₆) < (NH₄ClO₄, NH₄BF₄, TEAClO₄, TMABF₄) < (NH₄NO₃, KNO₃, TEANO₃, TMANO₃), that is, PF₆⁻ < ClO₄⁻ ≈ BF₄⁻ < NO₃⁻. Additionally, in the presence of identical anions, the bulky tetraalkylammonium ions (TMA⁺ and TEA⁺) shift the onset potential to a more positive position. These observations are very consistent with previous studies involving nanoparticle self-assembled monolayers with dithiols.^{1b} The

TABLE 1: Variation of Onset Potentials (E_{on} , V) and C8PyAu-1 Nanoparticle (Effective) Capacitance (C_{MPC} , aF) with Electrolyte Ions in Aqueous Solutions

electrolyte	E_{on} (V)	C_{MPC} (aF)
TBAP ^a		0.55
NH ₄ PF ₆	-0.06	1.23
KPF ₆	-0.04	1.19
TEAPF ₆	0	1.21
NH ₄ ClO ₄	0.05	1.32
NH ₄ BF ₄	0.10	1.32
TEAP	0.08	1.30
TMABF ₄	0.12	1.31
NH ₄ NO ₃	0.16	
KNO ₃	0.18	
TEANO ₃	0.20	
TMANO ₃	0.22	

^a In dichloromethane containing 0.10 M TBAP.

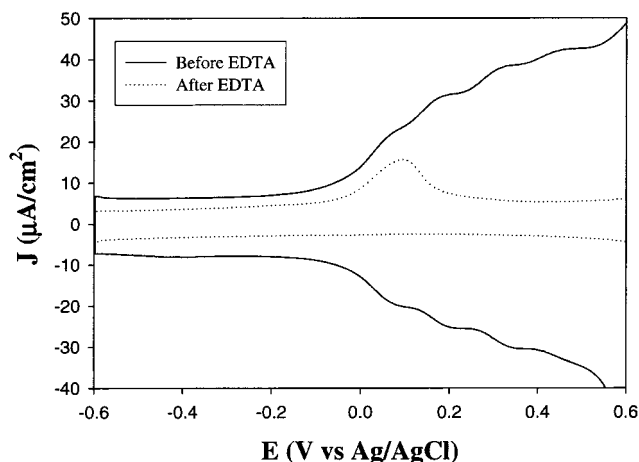


Figure 3. Differential pulse voltammograms (DPVs) of the gold nanoparticle monolayers as described in Figure 2 before and after immersion into 0.05 M EDTA for 3 h. The electrolyte solution is 0.10 M KPF₆. Other experimental parameters are the same as in Figure 2.

fundamental mechanism involved is equivalent to the effects of specific adsorption on the electrode double layer where the potential of zero charge shifts cathodically (anodically) with the adsorption of hydrophobic anions (cations) onto the electrode surface.⁷

The above nanoparticle surface assemblies can be easily removed by strong complexing reagents such as EDTA and reassembled using the same procedure (Scheme 2). Figure 3 shows the DPVs of a gold nanoparticle monolayer before and after EDTA treatment. One can see that, upon the treatment with EDTA, the discrete charging features of nanoparticles vanish into featureless responses that are characteristic of classical double-layer charging at an organic-coated surface. The electrode can then be reused to construct the nanoparticle assemblies.

The above observations demonstrate that the voltammetric responses of nanoparticle surface organized assemblies might behave like conventional molecular diodes or single-electron current rectifiers depending on the “softness” of the specific electrolyte ions. Thus, one can envision that, by manipulating the nature of the electrolyte ions, the nanoscale electron transfers might be quantum-like or bulklike.

Ion–MPC Pairing. The above ion–MPC pairing mechanism is further supported by the observation that the voltammetric profiles shift cathodically (anodically) with increasing concentrations of the hydrophobic anions (cations),¹

$$E_f = E^{o'} + \frac{RT}{n_a F} \ln \frac{K_2}{K_1} - (p - q) \frac{RT}{n_a F} \ln [\text{anion}] \quad (1)$$

where E_f and $E^{o'}$ are the formal potentials in the presence and absence of ion binding, respectively, n_a is the (effective) number of electron transfer, K_1 and q (K_2 and p) are the equilibrium constant and the number of anions bound to the reduced (oxidized) forms of the MPC molecules, respectively, and other parameters have their usual significance. Figure 4A shows a series of DPVs of a gold nanoparticle monolayer in solutions with varied concentrations of NH₄PF₆ (the solution ionic strength is maintained at 0.1 M by using NH₄NO₃). One can see that the voltammetric profiles shift cathodically with increasing concentration of PF₆⁻, as dictated by eq 1. Figure 4B depicts the variation of the peak potentials with PF₆⁻ concentrations, where one can see a very good linear regression for all of the charging peaks. However, the slopes are somewhat larger than -25 mV as predicted by eq 1 ($n_a = 1$ and $T = 298$ K) for a 1:1 ratio between the nanoparticle charge state and number of MPC-bound ions: -41 mV ($z = +1$); -45 mV ($z = +2$); -48 mV ($z = +3$); -52 mV ($z = +4$). The deviation becomes somewhat larger at higher charge states, indicating that electrostatic interactions might play a bigger role in the ion–MPC pair formation when the particles carry more charges. Also, the deviation is greater than that with nanoparticle self-assembled monolayers linked by alkanedithiols.¹ For instance, using the same electrolyte solutions with a monolayer of C6Au nanoparticles linked by 1,6-hexanedithiols, the corresponding slopes were found at -28 mV ($z = +1$), -35 mV ($z = +2$), and -41 mV ($z = +3$). This might be, at least in part, attributed to the particle-bridging Cu²⁺ ions that also facilitate further adsorption of hydrophobic anions. The contributions from these metal centers become less significant at higher charge states of the nanoparticles.

In the case of hydrophobic cations, the responses are quite complex. Figure 4C shows a series of DPVs of the same nanoparticle monolayers bridged by pyridine/Cu²⁺/pyridine chemistry in varied concentrations of TEANO₃ (again, with NH₄NO₃ to maintain the solution ionic strength at 0.1 M). As observed before,^{1b} the DPV profiles shift anodically with increasing concentration of TEA⁺, indicating adsorption of cationic TEA⁺ to the surface-bound particles. However, the associated binding process appears to be much more complicated than the case with nanoparticle assemblies linked by dithiol bridges.¹ Figure 4D depicts the variation of the onset potential with the concentration of TEA⁺. One can see that the slope of E_{on} vs $\ln[\text{TEA}^+]$ within the concentration range of 0.005–0.025 M is about +87 mV, significantly larger than that (+20 mV) found at higher concentrations (0.025–0.1 M). This suggests that at low concentrations the binding of hydrophobic cations to surface-bound nanoparticles is very sensitive to electrolyte concentrations whereas at high concentrations the binding appears to reach a saturated state. In contrast, previously, using dithiol-linked nanoparticle assemblies, we observed a linear profile of E_{on} vs $\ln[\text{TEA}^+]$ within the entire concentration range of 0.005–0.1 M (with the corresponding slope of +56 mV).¹ This appears to suggest that at low concentrations, the positively charged metal centers (Cu²⁺) even facilitate the binding of hydrophobic cations to the nanoparticle thin films despite their repulsive interactions. While the details involved are not clear at the moment, it is possible that charge screening by counter-anions will have to be involved.

MPC Capacitance. Because these voltammetric charging peaks reflect a series of single electron transfers, the C8PyAu-1 nanoparticle molecular capacitance (C_{MPC}) can be evaluated

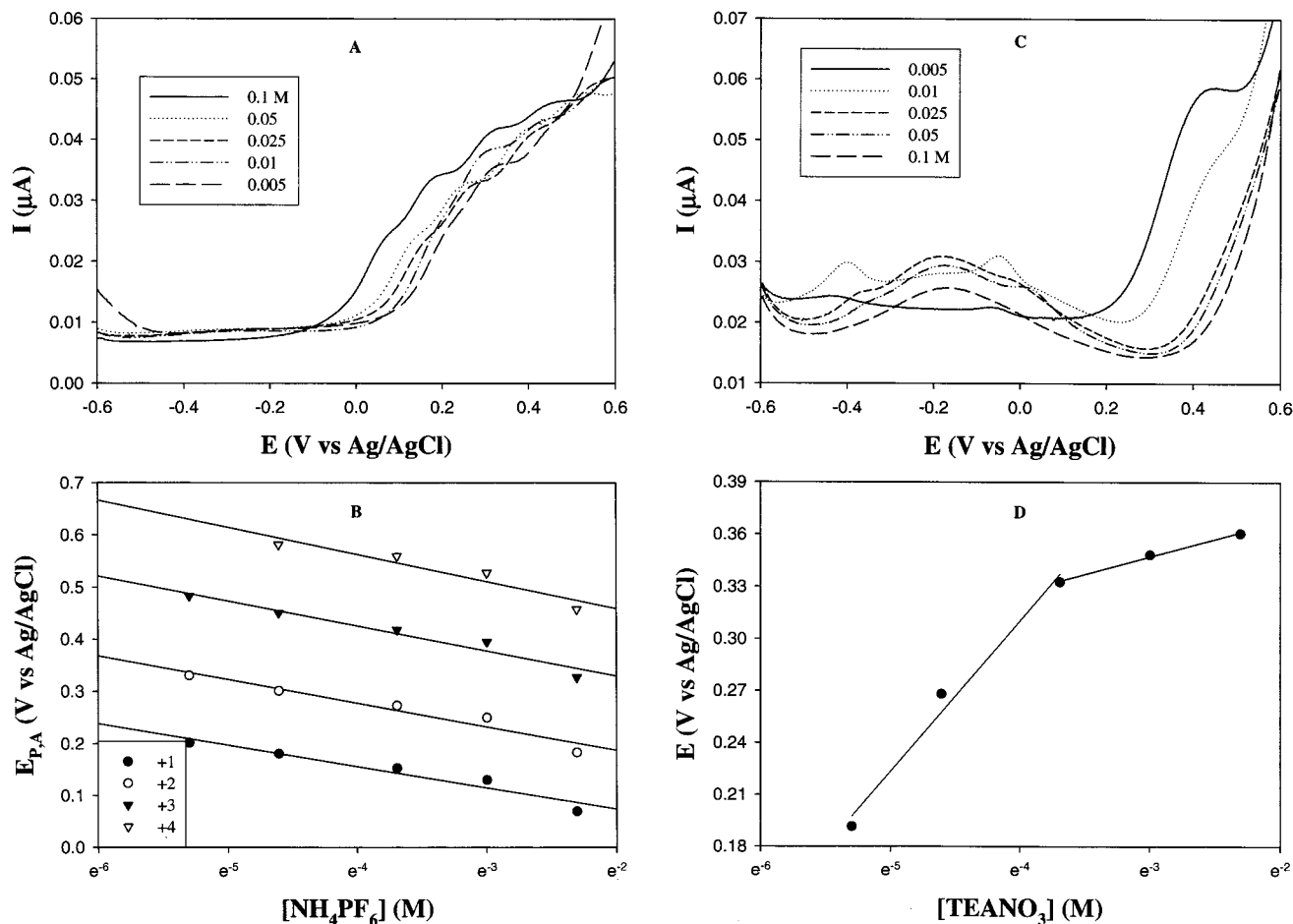


Figure 4. DPVs of the gold nanoparticle monolayers as described in Figure 2 in electrolyte solutions of varied compositions: (A) x M NH_4PF_6 + $(0.1 - x)$ M NH_4NO_3 ; (C) x M TEANO_3 + $(0.1 - x)$ M NH_4NO_3 . The values of x are listed in the respective figure legends. Panels B and D depict the respective variations of voltammetric peak potentials or onset potentials with the concentration of “soft” electrolyte ions. Symbols are experimental data, and lines are the corresponding linear regressions.

from the potential spacing (ΔV) between the neighboring peaks, $C_{\text{MPC}} = e/\Delta V$. The results are summarized in Table 1, along with the value calculated when the particles are dissolved in organic media (CH_2Cl_2). One can see that when the particles are dispersed in CH_2Cl_2 , the molecular capacitance is 0.55 aF, which is only slightly larger than that of C8Au particles prior to exchange reactions with ligand **1** (0.53 aF), indicating a very similar protecting monolayer structure. When the nanoparticles are immobilized onto electrode surfaces, the effective capacitance is much larger in aqueous solutions, 1.2–1.3 aF. This is, at least in part, attributed to the ion-binding properties that increase the effective dielectric constant of the MPC protecting monolayers, akin to the case where the MPC capacitance increased severalfold when the peripheral ferrocene moieties were oxidized to ferrocenium.⁸ Additionally, overall, in the same electrolyte solutions, the particle capacitance values are much larger (~50%) than those measured with MPC surface assemblies linked by alkanedithiols.¹ Again, this is partly attributable to the presence of peripheral metal ion centers (Cu^{2+}) that facilitate further binding of electrolyte ions (*vide ante*).

Conclusions

This report demonstrates that gold nanoparticle surface assemblies linked by pyridine/ M^{2+} /pyridine can be constructed with the thin film thickness readily controlled by the repetition of alternate dipping cycles. It is found that the associated nanoparticle quantized charging can be rectified in the presence

of some unique hydrophobic electrolyte ions, which is interpreted on the basis of an ion-binding mechanism. In addition, these molecular diode-like responses evolve from a conventional to quantized character with increasing hydrophobicity of the electrolyte ions. The presence of positively charged metal ion centers appears to facilitate further binding of hydrophobic electrolyte ions (anions and cations). Also, preliminary studies show that despite a longer tunneling distance than that with nanoparticle assemblies by dithiol linkages, the metal ion centers seem to enhance the electron-transfer kinetics of nanoparticle quantized charging. Further studies are currently underway.

Acknowledgment. This work was supported by the National Science Foundation (CAREER Award), the Office of Naval Research, the ACS Petroleum Research Fund, the Illinois Department of Commerce and Community Affairs, and the SIU Materials Technology Center. S.C. is a Cottrell Scholar of Research Corporation.

Supporting Information Available: Synthetic procedure and ¹H and ¹³C NMR characterizations of 4-(1,4,7-trioxo-9-mercaptononyl)pyridine and 4-(1-oxo-7-mercaptohexyl)pyridine. This information is available free of charge on the Internet at <http://pubs.acs.org>.

References and Notes

- (1) (a) Chen, S. *J. Am. Chem. Soc.* **2000**, *122*, 7640. (b) Chen, S.; Pei, R. *J. Am. Chem. Soc.* **2001**, *123*, 10607.

- (2) Chen, S. *J. Phys. Chem. B* **2000**, *104*, 663.
- (3) For instance, see: (a) Zamborini, F. P.; Hicks, J. F.; Murray, R. *W. J. Am. Chem. Soc.* **2000**, *122*, 4515. (b) Chen, S.; Murray, R. W. *J. Phys. Chem. B* **1999**, *103*, 9996. (c) Grabar, K. C.; Smith, P. C.; Musick, M. D.; Davis, J. A.; Walter, D. G.; Jackson, M. A.; Guthrie, A. P.; Natan, M. J. *J. Am. Chem. Soc.* **1996**, *118*, 1148. (d) Baum, T.; Bethell, D.; Brust, M.; Schiffrin, D. J. *Langmuir* **1998**, *14*, 866. (e) Peschel, S.; Schmid, G. *Angew. Chem., Int. Ed. Engl.* **1995**, *34*, 1442.
- (4) (a) Brust, M.; Walker, M.; Bethell, D.; Schiffrin, D. J.; Kiely, R. *J. Chem. Soc., Chem. Comm.* **1994**, 801. (b) Whetten, R. L.; Shafiqullin, M. N.; Khoury, J. T.; Schaaff, T. G.; Vezmar, I.; Alvarez, M. M.; Wilkinson, A. *Acc. Chem. Res.* **1999**, *32*, 397. (c) Templeton, A. C.; Wuelfing, W. P.; Murray, R. W. *Acc. Chem. Res.* **2000**, *33*, 27.
- (5) (a) Chen, S. *Langmuir* **2001**, *17*, 2878. (b) Maye, M. M.; Zheng, W.; Leibowitz, F. L.; Ly, N. K.; Zhong, C.-J. *Langmuir* **2000**, *16*, 490.
- (6) Sauerbrey, G. *Z. Phys.* **1959**, *155*, 206.
- (7) Bard, A. J.; Faulkner, L. R. *Electrochemical Methods*, 2nd ed.; John Wiley & Sons: New York, 2001.
- (8) (a) Hostetler, M. J.; Green, S. J.; Stokes, J. J.; Murray, R. W. *J. Am. Chem. Soc.* **1998**, *118*, 4212. (b) Green, S. J.; Stokes, J. J.; Hostetler, M. J.; Pietron, J. J.; Murray, R. W. *J. Phys. Chem. B* **1997**, *101*, 2663.